Molecular Dynamics Simulation of Penetrant Diffusion in Amorphous Polypropylene: Diffusion Mechanisms and Simulation Size Effects

Thomas R. Cuthbert and Norman J. Wagner*

Center for Molecular and Engineering Thermodynamics, Department of Chemical Engineering, University of Delaware, Newark, Delaware 19716

Michael E. Paulaitis

Department of Chemical Engineering, Johns Hopkins University, Baltimore, Maryland 21218

Giovanni Murgia and Bruno D'Aguanno

CRS4, Via N. Sauro, 10, I-09123 Cagliari, Italy

Received June 25, 1998; Revised Manuscript Received May 24, 1999

ABSTRACT: Amorphous, atactic polypropylene structures, consisting of 125, 729, and 2197 monomer repeat units folded into periodic cells, were generated to study the effects of simulation size on the transport of small molecules in simulations of amorphous polymers. The diffusion coefficients and solubilities of three particles having different sizes representative of He, Ar, and CO_2 are calculated from 4 ns molecular dynamics simulations. A definite system size dependence is observed in the solubilities resulting from a bias against the formation of large cavities in the smaller structures. Surprisingly, this bias does not significantly affect the diffusivities of the penetrants in these structures despite their jumplike diffusive motion. We also find the characteristic length scale for the turnover from the anomalous to the diffusive regime to be insensitive to the simulation size but inversely dependent on penetrant size. This insensitivity to simulation size of the diffusivity and turnover is in contrast to that found for diffusion in systems that are either static or have percolating networks. This difference points to the importance of dynamic coupling between the penetrant motion and the thermal motion of the polymer matrix. A rigorous statistical analysis of different methods of extracting the penetrant tracer diffusivity from the molecular simulations emphasizes the value of using the van Hove correlation function for analyzing penetrant motion.

I. Introduction

Molecular dynamics (MD) simulations are increasingly employed as a tool for exploring the transport of small molecules in polymeric systems. This popularity arises from its ability to provide not only estimates of macroscopic properties of interest, such as the diffusivity and solubility from first principles, but also detailed molecular information regarding the mechanisms of transport. These simulations provide a link between polymer chain architecture and penetrant transport that can be employed in the rational design and optimization of separation membranes.[1−5]

Several studies have focused on the transport of small penetrants through a variety of glassy polymer systems where both penetrant solubility and diffusivity have been simulated.[6−20] The solubility is typically calculated by Widom's Test Particle insertion method[21,22] or a variation thereof,[23,24] while penetrant diffusivity is calculated from the mean square displacement in both full MD simulations[6−8,12,13,16−20] or transition state approaches.[9,15,25,26] In the transition state approach, the energy surface for the penetrant existing at regular points in the structure is mapped and local minima, or "cavities", identified. Energy barriers between adjacent energy minima are calculated and the heights are used to determine a jumping frequency for the penetrant in going from one cavity to another. In general, qualitative agreement between simulation and experimental values of the diffusion coefficient and the solubility are obtained; only in a few specific cases has reasonable quantitative agreement been seen for either quantity.[12,15,27] While tuning the polymer's force-field parameters can improve this agreement, it has also been demonstrated that the size of the polymer simulation itself[24] and the method of generation[28] can have nonnegligible effects as well on the calculated penetrant solubility in a polymer glass.

For solubilities, the distribution of energetically favorable sorption sites or cavities is strongly affected by the simulation size. Typical polymer simulations consist of a single chain "folded" into a central simulation box that is then periodically replicated. Thus, changing the system size not only changes the polymer molecular weight, and thus the density of chain ends, but also affects the chain topology.[29−31] Recent simulations in which a uniform Gaussian chain topology is ensured independent of simulation size have uncovered another subtle statistical effect.[24] Namely, the distribution of cavities broadens and shifts to unfavorable energies simply because smaller simulation sizes restrict the density fluctuations that can occur. Hence, smaller simulation sizes lack the larger cavities that dominate the calculated excess chemical potential. In contrast, the effect of simulation size on penetrant diffusivity has not been studied systematically, primarily due to computational limitations. This effect is the focus of the work presented here.

The diffusion coefficient, D, is typically calculated from the mean square displacement of a penetrant with time. In the limit of long times, Fickian diffusion is

* Corresponding author. E-mail wagner@che.udel.edu.

10.1021/ma980997e CCC: $18.00
Published on Web 07/07/1999

achieved and

$$\lim_{t\to\infty}\langle r^2\rangle = 6Dt \tag{1}$$

where $|r(t) - r(0)|$, is the position of the penetrant at time t relative to its position at time $t = 0$. For diffusion in polymers, the mean square displacement of the penetrant is observed to pass through three distinct regimes.[32] The first is a short-time ballistic regime. A regime of anomalous diffusion follows in which the mean square displacement (MSD) is proportional to t^x with $x < 1$. Finally, for sufficiently long times, the penetrant enters a Fickian diffusive regime for which the MSD is proportional to t, as given by eq 1. The turnover from anomalous to Fickian diffusion is of particular interest, as it has been observed to occur typically when the MSD is approximately equal to the square of the length of the simulation box.[9,15] This coincidence of the MSD at turnover with the box length suggests that the Fickian diffusivities are box size dependent. It is hypothesized that once a penetrant has, on average, traveled multiple box lengths and is diffusing though multiple periodic images of the polymer, Fickian-like diffusion can be artificially induced, which may not reflect true Fickian diffusion of the penetrant within the bulk polymer.[25,33]

Weber and Paul[33] reported a simulation size effect on this turnover point in percolating structures of static polymer systems in which both the penetrant and the polymer are represented by the bond-fluctuation model. For systems below a critical box size, they found the turnover point to occur consistently at a MSD corresponding to their simulation box size and the calculated diffusion coefficient to decrease with increasing box size. Once a critical box size was exceeded, both the diffusion coefficient and turnover point became independent of box size. The authors deduced that truncation of the percolating pathway for penetrant diffusion at lengths shorter than the natural turnover length artificially induces Fickian diffusion at this new length scale of periodic replication. In contrast, simulations of diffusion in regular periodic structures do not show a size effect as periodic replication of a regular periodic structure does not induce any new length scale in the system.[34]

One important difference between these models with percolating channels and glassy polymers is that penetrant motion in glassy polymers is mediated by the polymer thermal motion. It has been shown that this thermal motion is required for penetrants to move between energetically favorable sites (cavities).[35] It is unclear whether percolating structures with no energetics will accurately capture the true mechanism of penetrant diffusion within polymer glasses. In this work, we examine the diffusion of three different penetrants in a molecularly detailed model of amorphous, atactic polypropylene via MD simulation. We examine both the detailed motion of the penetrants as well as calculate their transport properties and turnover points as a function of system size. Multiple methods of calculating the diffusion coefficient are analyzed to yield diffusivities, their uncertainties, and the molecular mechanism of diffusion.

II. Computational Methodology

A. Polymer Model. Polypropylene is modeled as a polymer chain of CH, CH_2, and CH_3 united atom groups. It is known that using this simplified model results in a larger diffusion coefficient than that for an all-atom representation.[7] However, as we are only interested in the relative transport characteristics of the penetrants in the polymer structures of different sizes, internal consistency suffices. This approximation enables the larger simulation sizes and longer run times required for the work proposed here.

Table 1. Number and Sizes of Polypropylene Structures and Penetrants Used in This Work

polymer size	number of atoms	simulation box length (Å)	number of structures	penetrant density[a] particles/Å^3	total number of penetrants simulated
125mer	375	20.9494	10	2.18×10^{-4}	20
729mer	2187	37.7089	3	1.55×10^{-4}	25
2197mer	6591	54.4684	1	1.24×10^{-4}	20

[a] Penetrant−penetrant interactions are turned off.

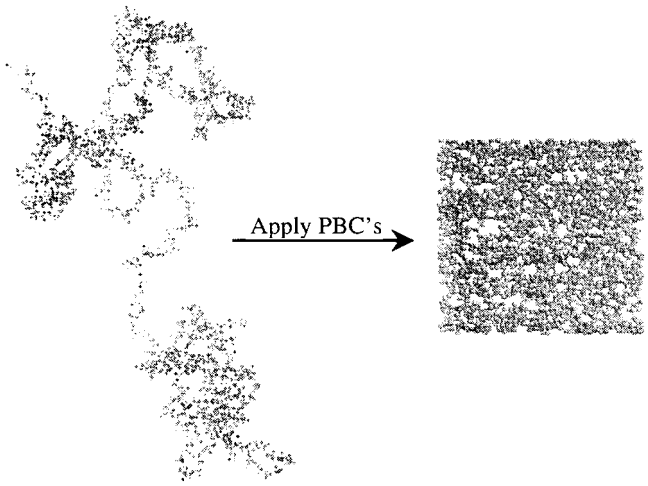

Figure 1. Unfolded and folded states of a 729mer, united atom model for polypropylene. Bead size is 25% of the van der Waals diameter.

Polypropylene chain lengths spanning more than an order of magnitude in molecular weight were studied. The polymer length in monomers, number of united atoms, the cubic simulation cell length, and the number of independent simulation runs of each size are listed in Table 1. Each simulation was performed on a periodic cell containing a single parent chain at a polymer density of 0.95 g/cm^3 with the average fraction of meso-dyads equal to 0.5. This choice of density is higher than that employed by others,[29,36] in part to avoid any long-lived (on the time scale of the simulation) percolating networks for the smallest penetrant. A typical parent chain is shown in Figure 1 in its folded and unfolded configurations. Initial configurations for the polymer glasses were generated using the Gaussian lattice algorithm.[31] We note that this algorithm ensures that the chain is Gaussian on all relevant length scales independent of simulation size. Each polymer was subjected to the same annealing schedule to generate the relaxed polymer chain used for subsequent simulation and analysis. This schedule entailed energy minimization of the initial configurations to mechanical equilibrium at 0 K to remove high-energy overlaps and distorted bond lengths and angles. Molecular dynamics was then performed at 1000 K for 200 picoseconds to remove any residual effects of the original lattice generation method and was followed by equilibration at 233 K for 300 ps.

Since the proper (Gaussian) chain topology is generated in the Gaussian lattice algorithm, polymer annealing is used only to relax the local chain environment.

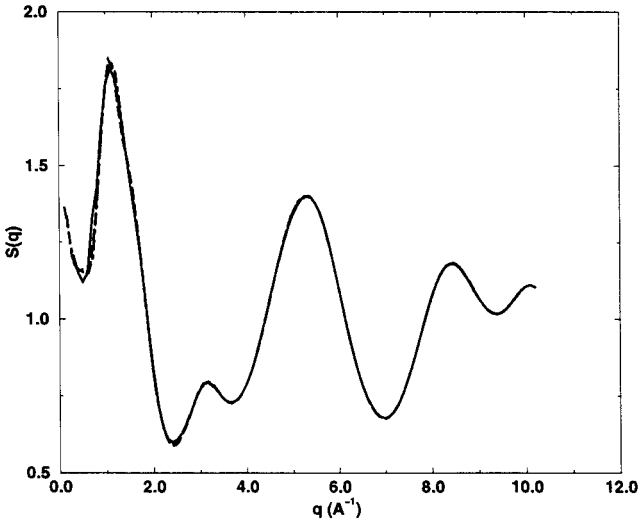

Figure 2. X-ray structure factors for the three polypropylene structure sizes averaged over the total number of configurations given in Table 1. 125mer (—), 729mer (- - -), and 2197mer (- — - —).

These include relaxation of distorted bond angles and bond lengths, as well as nonbonded van der Waals interactions. At the end of the annealing schedule, the three polymer chain lengths yield essentially identical X-ray structure factors, as seen in Figure 2. Note that these X-ray structure factors are calculated for the united atom model and, as such, do not have explicit hydrogens in the calculation. The momentum transfers of the first few minima and maxima are in good quantitative agreement with those calculated from simulations by Fukuda and Kuwajima[19] and Sylvester et al.,[36] as well as the experimental values reported therein.

Proof of glassy behavior is a complex question of time scales, aging, and sample preparation (see, for example, Sylvester et al.[36]). For our purposes, it is sufficient to demonstrate that no significant polymer motion or bond rotation occurs on the time scales over which penetrant diffusion is simulated. Note that our simulations are well below the glass transition temperature of the pure polymer and at a higher density. The average root-mean-squared displacement of the united atoms comprising the polymer, with and without the penetrants present, is ~3.3 Å after 4 ns, showing no significant motion of the polymer. Further, the torsional angles are observed to "wiggle" only about 20−30° around their initial values, without any trans−gauche or gauche−gauche rotations observed. Thus, we believe our simulations to represent diffusion in a glassy amorphous polymer.

Following the equilibration, the penetrants were inserted into pre-existing cavities within the polymer structure such that no two penetrants were closer than 8 Å. These structures were reequilibrated for an additional 50 ps and followed by production runs of 4 ns. All simulations were performed at a fixed volume and constant number of components, with simple velocity rescaling to approximate a constant temperature (±10 °C for the larger structures and ±20 °C for the 125mers). Additionally, the penetrant−penetrant interactions were set to zero during the production runs to prevent clustering. The timestep was 2 fs.

We used the force field expressions and parameters from AMBER 4.1 for bond stretching, bond angle bending, torsion angle rotation, and van der Waals nonbonded interactions.[37] Our own parallel MD algorithm, developed and validated in-house, was used to perform the simulations. The algorithm uses the force decomposition method[38,39] to distribute the MD calculations among multiple processors. The algorithm was checked against short runs of the AMBER 4.1 *sander* module and found to yield identical results with a significant speedup in time over the replicated data parallelization implemented there. The force decomposition algorithm allows us to simulate the larger structures efficiently for the 4 ns production runs on the parallel architecture of an IBM SP-2.

Table 2. Summary of Lennard−Jones (LJ) parameters for penetrant gases.[a]

penetrant	LJ ϵ (Kcal/mol)	LJ σ (Å)
He	0.0203	2.580
Ar−He	0.0203	3.405
CO_2−He	0.0203	4.468
SF_6−He	0.0203	5.510

[a] The mass for all three particles was fixed at 4.0 g/mol. All LJ parameters were taken from ref 40.

Table 3. Summary of Mean Values of μ^{ex} (kcal/mol) for Four Penetrants in the Three Different Structure Sizes[a]

polymer size	helium	Ar−He	CO_2−He	SF_6 −He
125mer	0.85 (0.04)	1.17 (0.11)	1.68 (0.42)	3.03 (1.62)
729mer	0.84 (0.01)	1.11 (0.03)	1.37 (0.10)	1.61 (0.29)
2197mer	0.84 (0.006)	1.11 (0.02)	1.35 (0.06)	1.48 (0.12)

[a] Values in parentheses are the standard deviations for the distributions.

B. Penetrant Model. In addition to studying the effect of polymer simulation size on penetrant diffusion, we also examine the effect of changing the penetrant size. However, to limit the number of variables in this study, we choose to examine helium and hypothetical derivatives "argon−helium", Ar−He, and "carbon dioxide−helium", CO_2−He. These derivatives have the same mass and Lennard-Jones (LJ) well depth as helium,[40] but retain their nominal LJ diameter, σ, thus allowing the study of penetrant size. Table 2 summarizes the penetrant LJ parameters.

III. Results and Discussion

A. Size Effects from Solubility Calculations. In previous work,[24] we demonstrated a system size dependence of the solubility of simple gases in glassy polystyrene. The size effect is manifested as a skewing of the distribution of the excess chemical potentials with a shift in the mean to higher values. The origin of this size effect is a bias against formation of larger cavities within the smaller structures. Using methods described in this previous work,[24] the polypropylene structures studied here were checked for a cavity bias. The distributions of the excess chemical potentials are shown in Figure 3 with their mean values summarized in Table 3. Despite the similar X-ray scattering profiles in Figure 2, the 125mer shows a much lower and broader distribution than the two larger polymers. For both He and Ar−He, the distributions are reasonably symmetric about the mean and yield the same value for the mean independent of polymer simulation size. For CO_2−He in the 125mers, the distribution is skewed somewhat to higher values compared to the two larger polymers. This small difference indicates that cavities the size of

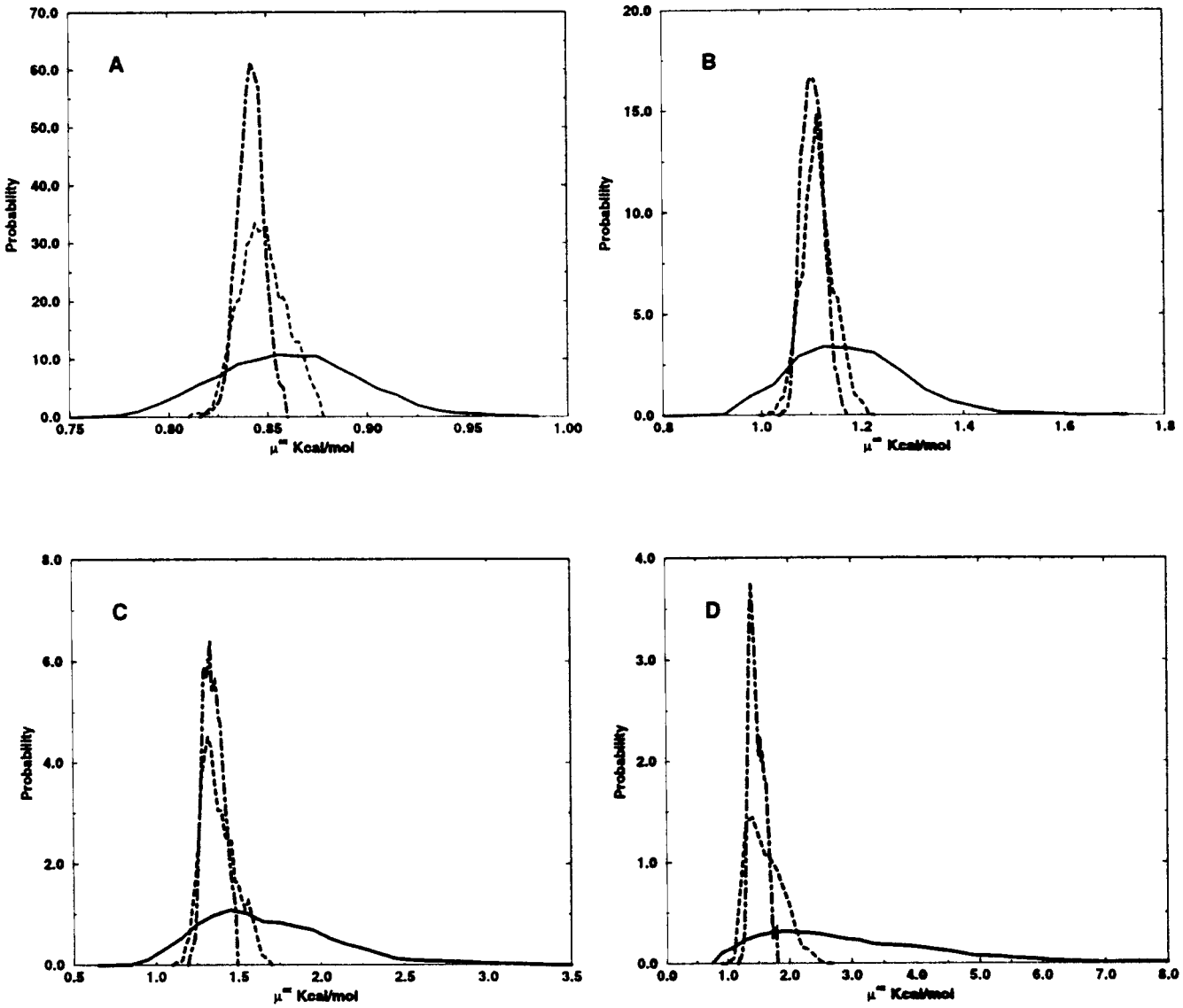

Figure 3. Distributions of μ^{ex} for (A) He, (B) Ar−He, (C) CO_2−He, and (D) SF_6−He in the different polymer structure sizes. The distributions were calculated from the last 100 ps of the MD equilibration runs. Distributions are averaged over all structures for a given polymer size: 125mer (—), 729mer (- - -), and 2197mer (- — - —). The distributions are normalized so $\int P(\mu^{ex})\, d\mu^{ex} = 1$.

the CO_2−He LJ diameter (4.48 Å) and larger are not as prevalent in the 125mers. Further evidence for this bias is seen by examining the solubility of SF_6−He (LJ diameter = 5.51 Å). Here the distribution of the excess chemical potential is skewed toward significantly higher values with a correspondingly higher mean value, thus indicating that there are few cavities exceeding this size in the 125mers compared to the 729mers or the 2197mers.

The cavity bias can also be quantified by examining the cavity size distribution (CSD) for the three polymers shown in Figure 4. The CSD was calculated by placing a grid with 0.1 Å between nodes in the structure and by calculating the largest hard sphere that could be placed at that point without overlapping the van der Waals radii of neighboring polymer atoms. These cavity size distributions are normalized such that the probability of inserting a point particle into the polymer is 1. We see no significant difference between the two larger polymers; however, the 125mers show a narrower distribution. The effect of this narrower distribution on the diffusion coefficient is examined in detail in section D.

B. Size Effects on Thermal Control. For this work, simple velocity rescaling for all atoms was used to maintain an approximately constant temperature during the simulations. It is well-known that fluctuations within a system scale inversely with the square root of the number of atoms in the system. For the 125mers with a ±10 °C thermostat, temperature fluctuations required rescaling approximately every 20 time steps. It was found that this frequent rescaling led to anomalous heating of the penetrants. The penetrant velocity distribution, as shown in Figure 5a, has a Maxwell−Boltzmann form with a best fit temperature of 262 K, approximately 30 K above the specified set point. However, the polymer itself was maintained at the correct temperature, as shown by its velocity distribution plotted in Figure 5b. We note that this phenomenon is not limited to our implementation of the MD algorithm and is similar to the "cold solute/hot solvent problem"[41] seen in protein simulations. In the larger polymers, where the frequency of velocity rescaling is much less (approximately 1 in 1000 steps in the 729mer and 1 in 200 000 steps in the 2197mer), both penetrants

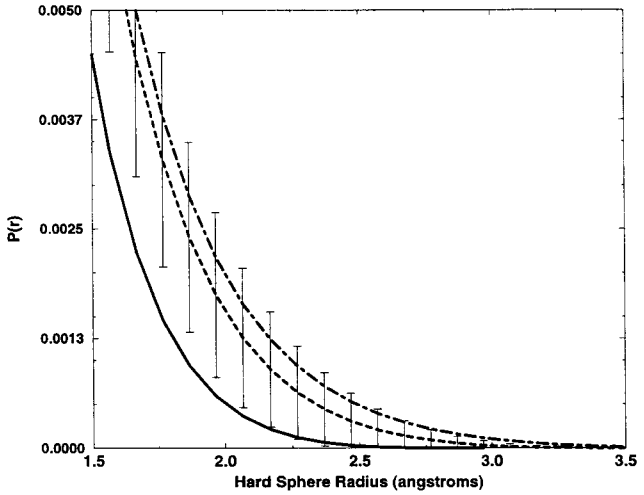

Figure 4. Cavity size distribution as probed by hard spheres. $P(r)$ is the normalized probability of finding a cavity of radius r. $P(r)$ is normalized such that the probablitiy of inserting a point particle is 1.0: 125mer (—), 729mer (- - -), and 2197mer (- — - —). Typical error bars are given for the 729mer.

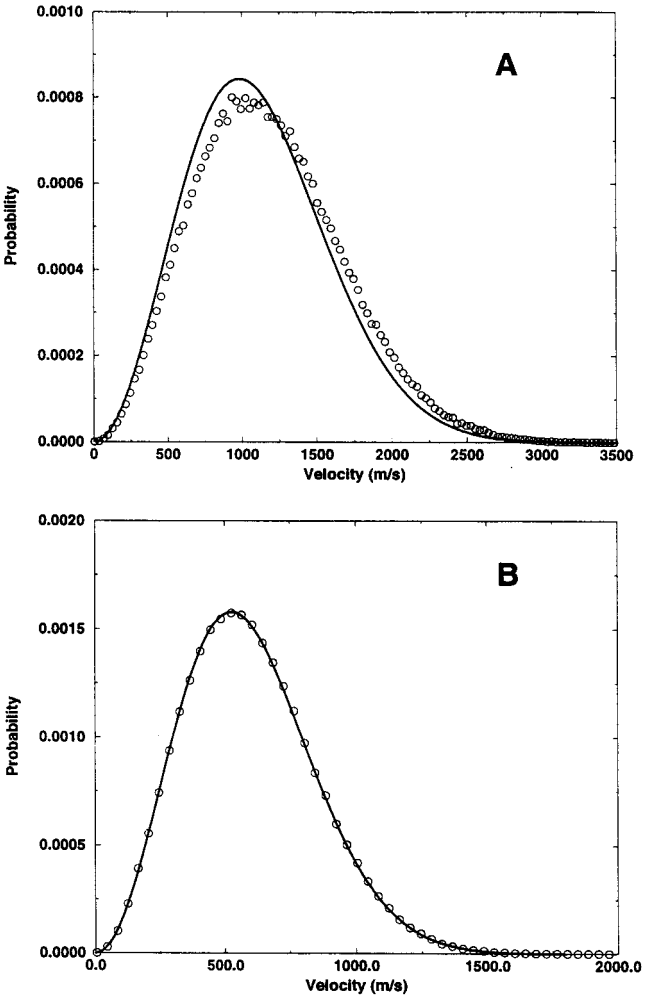

Figure 5. Velocity distribution of (A) Ar—He penetrants and (B) polymer atoms, from a 4 ns simulation of Ar—He in a 125mer with a ±10 °C thermostat. Lines show the Maxwell—Boltzmann velocity distribution at 233 K. The best fit of the Maxwell—Boltzmann velocity distribution for the penetrants is at 262 K, and best fit for the polymer atoms is at 233 K.

and polymer were maintained at the correct temperature, as reflected by their Maxwell—Boltzmann distributions. Note that this simulation artifact for a small system size will tend to increase erroneously the penetrant diffusion coefficient in the smaller polymers.

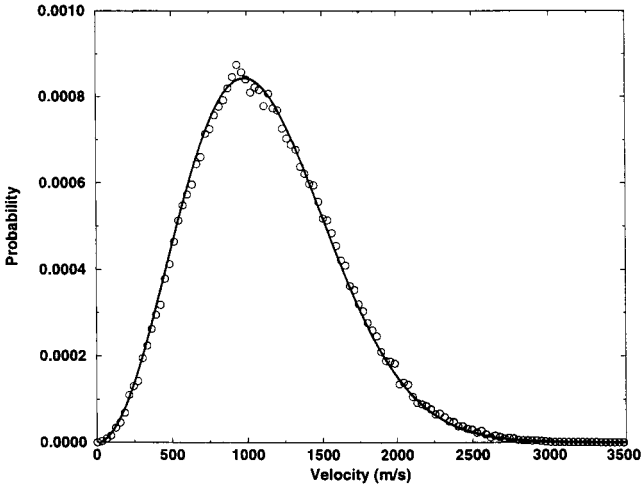

Figure 6. Velocity distribution for Ar—He penetrants in a 125mer with temperature rescaling occurring only when the temperature deviates by ±20 °C from the set point. Open circles are the velocity distribution calculated from the simulations, and the solid line is the Maxwell—Boltzmann distribution at 233 K.

We attribute the poor temperature control of the penetrants in the smaller polymers to the fact that the simulations are essentially composed of two weakly coupled systems (polymer and penetrants). During a rescaling of velocities to heat the system, energy is injected into the system equally among all degrees of freedom (dof). However, the polymer dof are much stiffer (due to chemical bonds) and kinetic energy is dissipated more quickly than from the penetrant dof. Therefore, the polymer dof require more energy than do the penetrant dof, but as energy is partitioned equally among all dof, the penetrants become effectively "hotter." Likewise, when velocities are rescaled to cool the system, the "hot" penetrants will remain "hot" as the energy is again removed equally from all degrees of freedom of the system. For the smaller structures with inherently larger thermal fluctuations, the rescaling frequency for a ±10 °C criterion is higher than the penetrant thermal equilibration time, leading to anomalous penetrant heating. The effect can be exaggerated when velocity rescaling is forced to occur at every time step in the smaller structures; the velocity distribution of the penetrant shifts even higher to 277 K. Anomalously "hot" penetrants are not seen in the larger polymers, as there is sufficient time for the penetrants and the polymer to equilibrate thermally between rescaling. When velocity rescaling for the 125mers is done less frequently (through the use of a ±20 °C criteria), the correct velocity distribution is recovered, as seen in Figure 6. It was not practical to use separate thermostats for the polymer and penetrants, as there are too few penetrants in our simulations to generate accurate values of the average kinetic energy needed for the velocity rescaling. Therefore, for this work, we rely on the larger polymer to act as a thermal reservoir for the penetrants, and all production runs for the 125mers were rescaled when the instantaneous temperature deviated by more than ±20 °C from the desired temperature.

C. Calculation of the Diffusion Coefficient. Penetrant diffusion coefficients are calculated from the MD simulations by four different methods. The first and

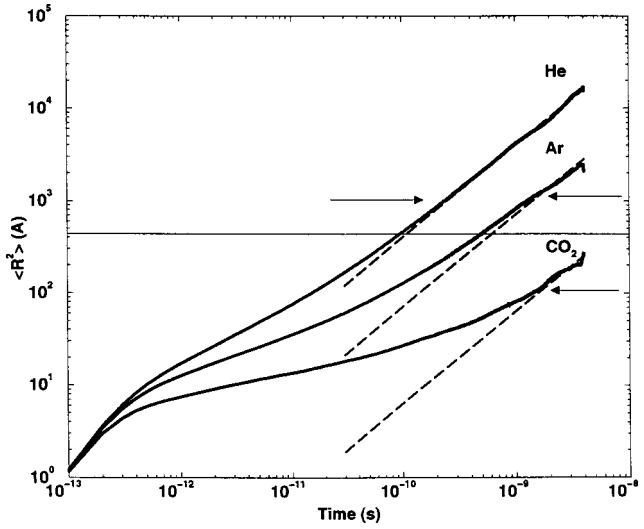

Figure 7. Mean square displacements for (A) He, (B) Ar−He, and (C) CO_2−He in the 125mers (solid lines). The dashed lines have slope 1, indicating that the diffusive regime has been reach as per eq 1.

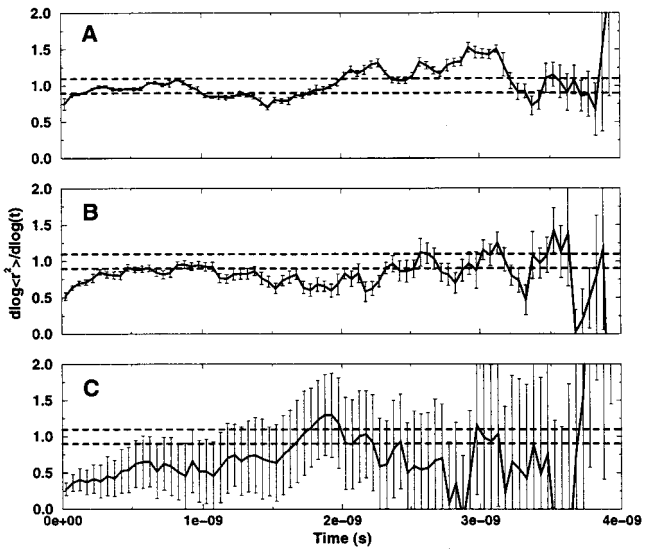

Figure 8. $d(\log\langle r^2\rangle)/d(\log t)$ for (A) He, (B) Ar−He, and (C) CO_2−He (solid lines) derived from the average mean square displacement s shown in Figure 7. The dashed lines are placed at 1.0 ± 0.1, indicating the turnover from the anomalous to diffusive regime.

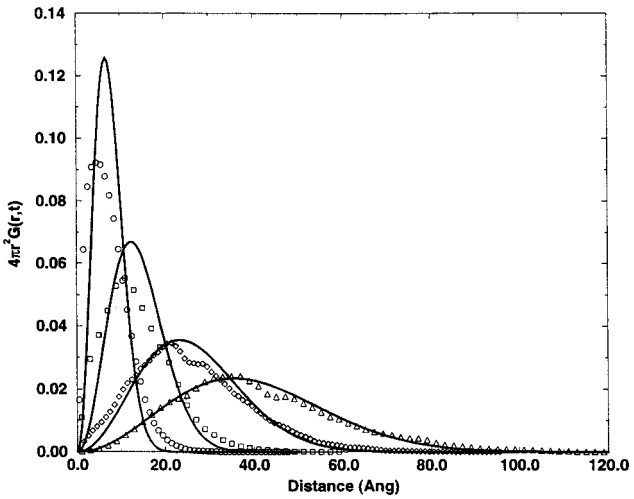

Figure 9. The van Hove self-correlation function for He averaged over the 125mers. 10 ps, ○; 50 ps, □; 200 ps, ◇; 500 ps, △. Symbols were calculated from the MD trajectory; the line is the best fit to the data from eq 4.

most commonly used method is to calculate the MSD of the penetrant, plot it versus time, and fit a line to this plot in the limit of long time (see eq 1). The MSD was calculated as a time correlation function of the penetrant positions starting at 100 fs intervals along the trajectory. Figure 7 shows typical curves for MSD versus time for the three different penetrants averaged over all 125mers. All three penetrants reach the diffusive regime as denoted by the dashed line of slope 1 on the log−log plot. As expected, the time required to reach the diffusive regime depends on the penetrant size: Helium reaches this regime first, followed by Ar−He, and finally by CO_2−He. Also included in this figure is a horizontal line representing the simulation box size squared. We see that the diffusive regime for helium is reached at roughly the same length scale as the box size, but for Ar−He the turnover appears to occur beyond this point, and for CO_2−He it occurs well inside the simulation box.

A second, closely related method of calculating the diffusion coefficient is to plot $d(\log\langle r^2\rangle)/d(\log t)$ versus time; the diffusive regime is reached when this derivative reaches a value of unity. The diffusion coefficient is then determined as an average of the instantaneous diffusion coefficient

$$D = \frac{1}{6}\frac{d\langle r^2\rangle}{dt} \tag{2}$$

This method allows for a more precise definition of the turnover from anomalous to Fickian diffusion; in this work we define the turnover to occur when $d(\log\langle r^2\rangle)/d(\log t) = 1 \pm 0.1$. Figure 8 shows $d(\log\langle r^2\rangle)/d(\log t)$ generated from the average MSDs for the three penetrants shown in Figure 7. The turnovers as determined by this method are shown in Figure 7 as arrows and are in agreement with the corresponding turnover obtained from the first method.

In the third method, the self part of the van Hove correlation function defined as

$$G_s(r,t) = N^{-1}\Big\langle \sum_{j=1}^{N} \delta\,[r + r_j(0) - r_j(t)]\Big\rangle \tag{3}$$

is compared with the known analytic form for Fickian diffusion. This function gives the probability that a penetrant moves a distance $|r|$ in time t. It has the limiting form:[42]

$$G_s(r, t) = (4\pi Dt)^{-3/2} e^{-r^2/4Dt} \tag{4}$$

$G_s(r, t)$ is constructed from the MD trajectories for the penetrants and fit using D as the only adjustable parameter. Figure 9 shows $G_s(r, t)$ constructed from the data for helium in the 125mers and the best fit to eq 4. Note that at short times ($t < 100$ ps), the agreement is poor as diffusion is in the anomalous regime. However, at longer times ($t > 100$ ps) the data and the expected form of $G_s(r, t)$ converge. These observations are consistent with the turnover derived from the previous methods.

The fourth method is related to the third in that the first four moments of the displacement, $\langle r_i^n\rangle$, are calculated from the van Hove correlation function and used

Table 4. Values of the Diffusion Coefficients for He, Ar−He, and CO_2−He in the Different Sized Structures Calculated by the Four Various Methods[a]

penetrant	structure	MSD	$d(\log\langle r^2\rangle)/d(\log t)$	fit $G(r,t)$	moments
He	125mer	6.8	6.8	6.7	6.5
	729mer	7.1	7.1	7.3	7.2
	2197mer	6.1	6.0	6.2	6.1
Ar−He	125mer	1.0	1.0	1.1	1.1
	729mer	0.9	0.9	0.85	0.9
	2197mer	1.2[b]	1.2[b]	1.2	1.2[b]
CO_2	125mer	0.12	0.10	0.11	0.11
	729mer	0.11	0.11	0.12	0.12
	2197mer	0.14	0.15	0.12	0.15

[a] All values of D in units of 10^{-5} cm^2/s. Error estimates (at 99.9% confidence) are ±3% in for He, ±15% for Ar−He, and ±22% for CO_2−He. [b] Values changed after statistical analysis, see the text for details.

to determine D.

$$\langle r\rangle = \int_0^\infty \frac{r}{8(\pi Dt)^{3/2}} e^{-r^2/4Dt}\, 4\pi r^2\, dr = \left(\frac{16Dt}{\pi}\right)^{1/2}$$

$$\langle r^2\rangle = \int_0^\infty \frac{r^2}{8(\pi\, Dt)^{3/2}} e^{-r^2/4Dt}\, 4\pi r^2\, dr = 6Dt$$

$$\langle r^3\rangle = \int_0^\infty \frac{r^3}{8(\pi\, Dt)^{3/2}} e^{-r^2/4Dt}\, 4\pi r^2\, dr = \frac{32}{\sqrt{\pi}}(Dt)^{3/2}$$

$$\langle r^4\rangle = \int_0^\infty \frac{r^4}{8(\pi\, Dt)^{3/2}} e^{-r^2/4Dt}\, 4\pi\, r^2\, dr = 60(Dt)^2 \quad (5)$$

When the penetrant motion becomes diffusive, the Gaussian form of the van Hove correlation function is valid and all four moments should yield the same value of D. An advantage of this method is that it emphasizes information from the center of the distribution about which the statistics are the best. Although not shown here, these moments converge for time scales longer than the turnovers determined by the previous three methods.

The values of the diffusion coefficients determined by all four methods are summarized in Table 4. The numerical values for He are reasonable, with typical values on the order of $(6-7) \times 10^{-5}$ cm^2/s, as found for helium in other glassy polymers and melts.[19,25,2] All four methods yield the same value for each polymer within numerical uncertainty. The only exception was for the original values of the diffusion coefficient of Ar−He in the 2197mer. Here the fitting of the van Hove correlation function to the data resulted in a higher value of the diffusion coefficient (1.7×10^{-5} cm^2/s). The reason is evident from inspection of Figure 10, where the van Hove correlation function and the fit to eq 4 are compared at long times. At large displacements, the Fickian model does not predict the high probabilities of $G_s(r, t)$. This is a consequence of two penetrants, which are found to be moving much faster and further than the other 18. Since all the methods for calculating D, except fitting $G_s(r, t)$, rely on averages of the square of the mean distance traveled, they will be skewed by penetrants showing accelerated diffusion. If these two penetrants in the 2197mer are excluded from the calculations, we recover the same diffusion coefficient ($D = (1.2 \pm 0.1) \times 10^{-5}$ cm^2/s) for all methods. The two trajectories with large MSD values are not a simulation error but rather a sampling artifact. They are valid

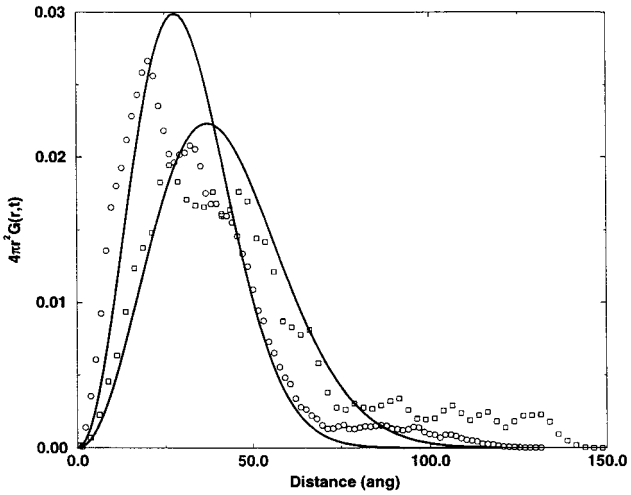

Figure 10. van Hove correlation function calculated from the MD trajectory of Ar−He in the 2197mer at 2000 ps (○) and 3000 ps (□). The lines are the best fit to eq 4.

Table 5. Turnover Time and Distances for He, Ar−He, and CO_2−He in the Three Different Structure Sizes[a]

		turnover	
penetrant	structure	distance (Å)	time (ps)
He	125mer	25.7 (2.7)	154 (48)
	729mer	31.3 (3.2)	255 (53)
	2197mer	29.3 (2.2)	195 (34)
Ar−He	125mer	19.9 (4.7)	470 (160)
	729mer	23.4 (5.6)	980 (140)
	2197mer	24.1 (5.1)	660 (130)
CO_2	125mer	9.5 (4.1)	1600 (272)
	729mer	9.8 (3.7)	1165 (244)
	2197mer	10.1 (3.4)	920 (203)

[a] Numbers in parenthesis represent error estimates. Box sizes for the three simulation sizes are as follows: 125mer, 20.9494^3 Å^3; 729mer, 37.7089^3 Å^3, 2197mer, 54.4684^3 Å^3.

trajectories; however, because of the limited number of penetrants simulated, their probability of occurrence, as given by $G_s(r,t)$, is small. The occurrence of even one such trajectory in a small population skews the results to yield a much higher diffusion coefficient. Thus, we perform a statistical analysis of the data to properly account for limited sample sizes.

As $G_s(r, t)$ is a normal distribution, the t-test is applied to the mean penetrant displacements over the time period for which the diffusion coefficient was calculated. With a 99.9% confidence interval, the "fast" penetrants in the Ar−He 2197mer simulation are found to have mean displacements outside that expected for penetrants obeying eq 4 (using $D = 1.7 \times$ cm^2/s) and can be excluded. The t-test was applied to all data sets and no other penetrants were rejected. After making this correction, we see no significant differences among the various methods for calculating D.

From the results in Table 4, we see a slight simulation size effect for helium. When increasing the box size to the 2197mer, a lower value of D is obtained. Moreover, this is the opposite of that observed for the other two penetrants. The larger two penetrants show a slight increase in diffusivity in the 2197mer compared to the smaller polymers. However, this difference is within the estimated uncertainty in the simulation data. To understand this, we now turn to the analysis of the turnover from anomalous to Fickian diffusion. Table 5 shows the turnover times and distances for each penetrant as a function of box size based on the analysis of

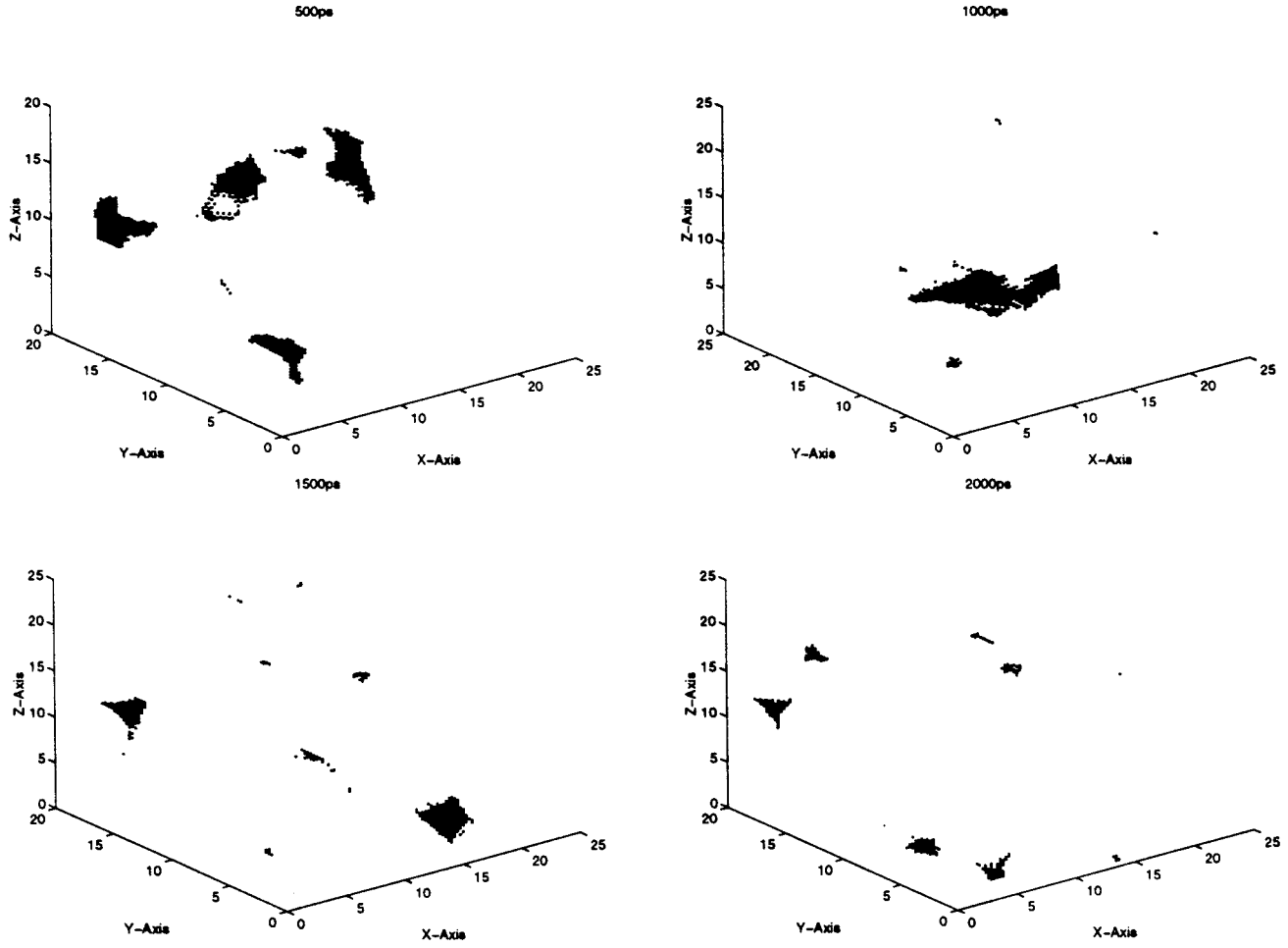

Figure 11. Accessible volume for Ar−He at different times during the simulation in a 125mer. The polymer has been removed for ease of visualization.

$d(\log\langle r^2\rangle)/d(\log t)$. With the exception of helium, all penetrants reach the diffusive regime before traveling a root mean square (rms) box length. This holds for all polymer simulation sizes.

It is also evident from the results in Table 5 that the effect of increasing the simulation size on the turnover distance is only modest and nearly within the simulation uncertainty. This is in contrast to what is seen in the percolating structures of the bond-fluctuation model and the transition state approach for diffusion, where both the value of D and the turnover distance are linear functions of simulation box length. This dependence on simulation size may be attributed to the static nature of the polymer and the periodic boundary conditions used in these techniques. In both methods, a single snapshot of the polymer is used for the diffusion calculations and the penetrants move from one fixed cavity to another. Thus, when the penetrant has traveled one box length in distance, it enters into a periodic image which is exactly like the one it just left. As the penetrant visits more of these identical periodic images, the effect of the artificial replication of the initial image is manifest in the turnover point and the calculated diffusion coefficient.[33]

In a full MD simulation, new cavities within the structures open and close due to the thermal motion of the polymer. As the penetrant travels through a simulation box and passes into a periodic image, this new image is sufficiently different from the last due to the local thermal motion of the polymer that the effect of the periodic boundary condition on the diffusivity and turnover point is ameliorated. This dynamic nature of the polymer is seen in Figure 11, where the accessible volume of Ar−He (i.e., regions in which there is no overlap of the LJ radius of the penetrant and the polymer atoms) is shown in snapshots separated by 500 ps for one of the 125mer structures. This time interval corresponds to the average time required for Ar−He to travel a rms distance equal to the 125mer box dimension. Clearly the penetrant sees an evolving local environment due to local thermal motion in the glassy polymer.

We also note that the turnover distance decreases with increasing penetrant volume and that the correlation is linear ($r^2 = 0.99$) with the particle volume (i.e., the $\sqrt{\text{MSD}}$ at turnover $\propto 1/\sigma^3$). Again, this is in contrast to what is seen for transition state models in which the turnover distance is insensitive to the penetrant volume.[9,15] Thus, while the simulation size has only a minor impact on the turnover and the diffusion coefficient, the $\sqrt{\text{MSD}}$ at turnover is inversely proportional to the penetrant volume, a phenomenon not seen in the transition state model.

D. Short Time Behavior. In previous work,[6,8,13,15,16,35] the mechanism of diffusion of small penetrants in polymer glasses has been identified as occurring through an activated/jumping mechanism. This proposed mechanism has been modeled using transition state theory to estimate the diffusivity of small particles in static

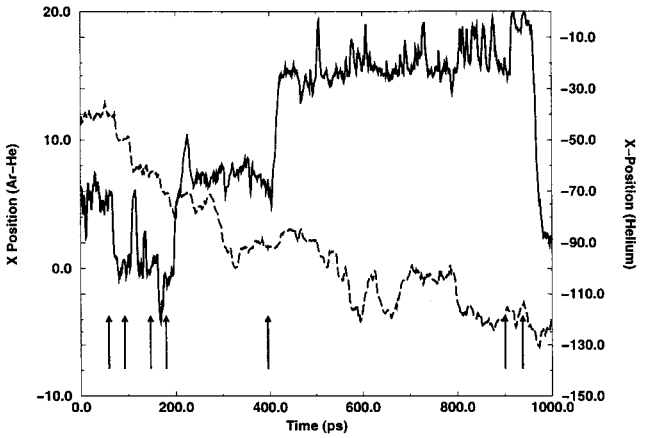

Figure 12. Jump map for Ar−He (solid line) in 125mer the arrows indicated the start of a jump event. The dashed line is the *X*-position for a He atom. Note the different scale between the two penetrants.

polymer structures.[9,15,25] If diffusion occurs only through an activated or jumping mechanism, the diffusion coefficient may be estimated by

$$D = \langle f \rangle \langle L \rangle^2 / 6 \qquad (6)$$

where f is the frequency of jump events, L is the jump distance, roughly the distance between centers of the two potential energy minima (cavities) involved in the jump event, and $\langle ... \rangle$ denotes the ensemble average. Note that in writing eq 6, the frequency of a jump event and the jump length are assumed to be uncorrelated, such that their ensemble averages can be computed independently.

We see a jumping mechanism here for the local penetrant motion. A jump is determined as follows: first, the penetrant position is averaged over a time interval such that the ballistic motion within a cavity is averaged out; in this work, we choose a 1 ps time interval. Second, the sign of the slopes of the *x*, *y*, and *z* components of the trajectory are followed. When a slope changes sign, the penetrant position is noted. When a slope changes sign again, the position is again noted and the distance the penetrant traveled between the two events calculated. If the distance is greater than an average cavity diameter of 5 Å, a jump event has occurred. Figure 12 shows a typical jump map for He and Ar−He in a 125mer.

Figure 13 shows the distribution of residence times (i.e., the time between jump events) for all penetrants in the three polymers. The distributions are quite broad, with tails extending out to hundreds of picoseconds. These broad distributions are indicative of a wide range of local environments within the polymer structure. We note that while the modes of the distributions are nearly the same, the distributions narrow somewhat as the polymer size increases. The narrowing is a consequence of the greater number of larger cavities in the larger polymers, which provide more suitable sites to which penetrants can jump, thus decreasing the time they are trapped within a single cavity.

Figure 14 shows the distribution of jump distances for the penetrants; Figure 15 shows the distribution of jump times (i.e., time between the start of jump and end of jump). Here we see no significant difference in the distributions for the different polymers. It is interesting that the distribution of jump times is similar for all

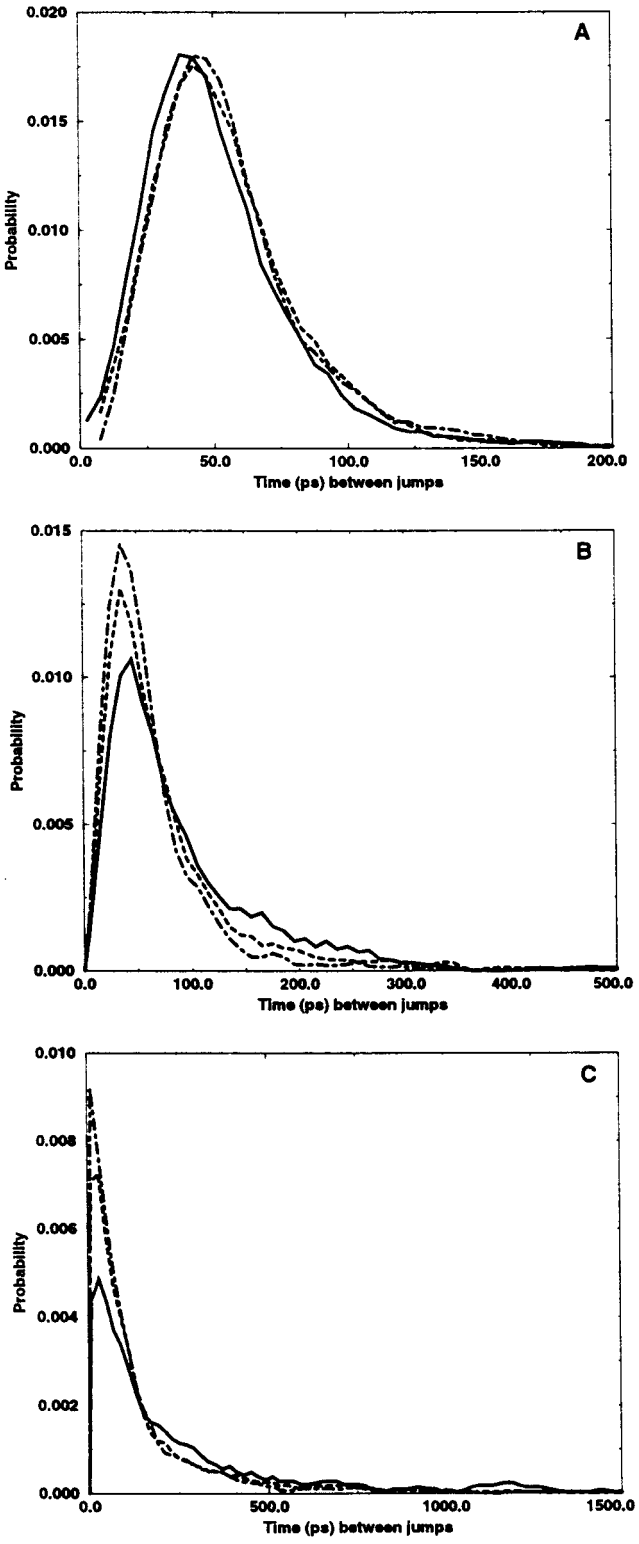

Figure 13. Distribution of residence times (times between jump events) for (A) He, (B) Ar−He, and (C) CO_2−He in the three different structures sizes: 125mer (—), 729mer (- - -), and 2197mer (- — - —).

penetrants and that the velocity during a jump event is much closer to the thermal velocity (ballistic motion) of a penetrant than the diffusive velocity.

The size effect evident in the solubility calculations and the CSD does not appear to affect significantly the diffusivity of the penetrants or the local, activated motion underlying the diffusive process. Although the cavity size distribution shows a bias against forming

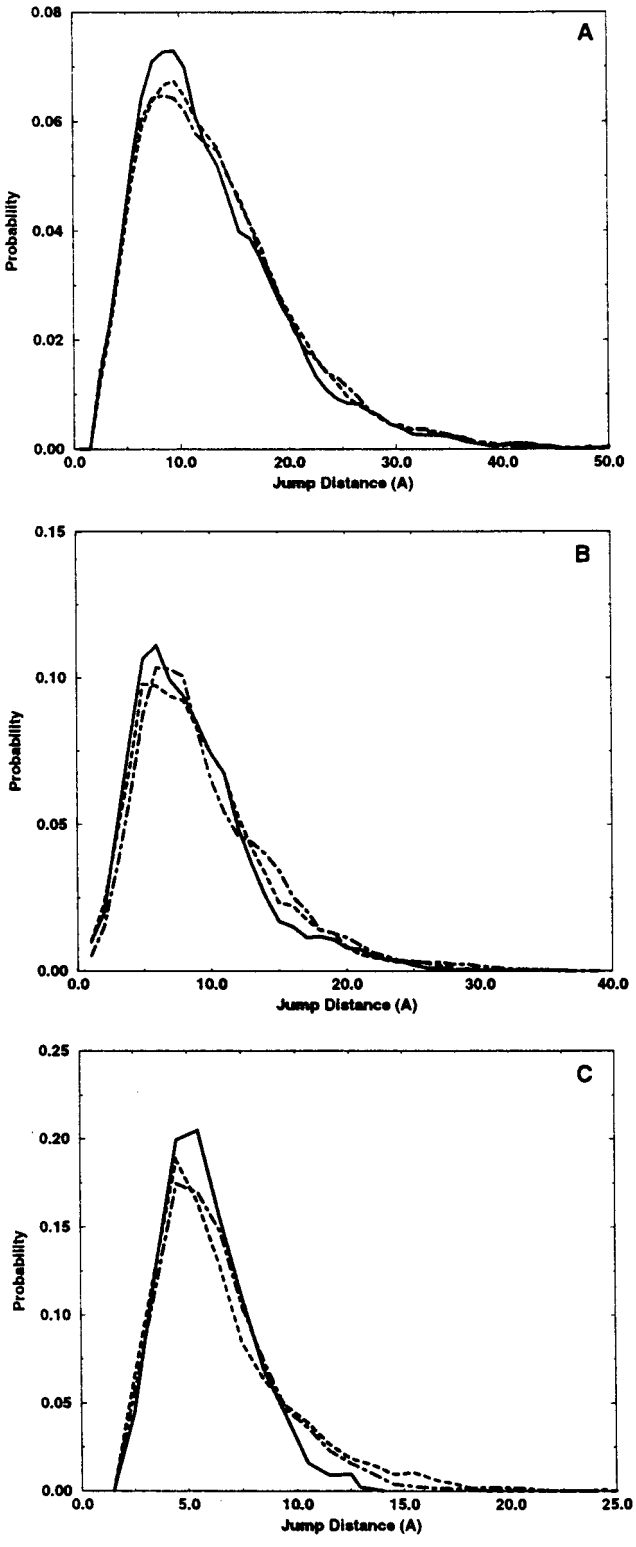

Figure 14. Distribution of jump distances for (A) He, (B) Ar−He, and (C) CO_2−He in the three different structures sizes: 125mer (—), 729mer (- - -), and 2197mer (- — - —).

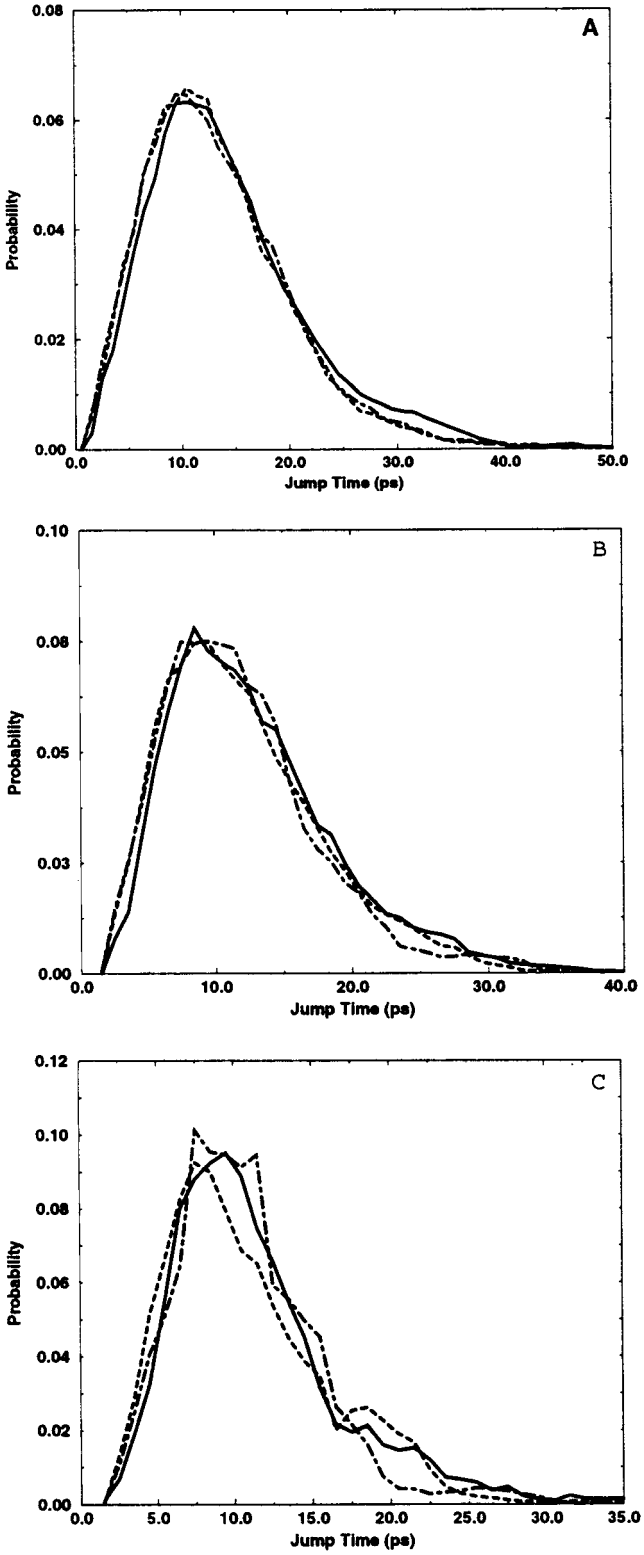

Figure 15. Distribution of jump times for (A) He, (B) Ar−He, and (C) CO_2−He in the three different structures sizes: 125mer (—), 729mer (- - -), and 2197mer (- — - —).

large cavities in the 125mers, the interaction of the penetrants with the polymer tends to reduce the bias as the very presence of the penetrants will tend to create larger cavities in the small structures.

The values of the diffusion coefficients calculated directly from the penetrant trajectories using the moment method are compared directly with those estimated from transition state theory (eq 6) and our results presented in Figures 13−15. To determine the jump frequency, we use the average jump time plus the average residence time, and for the mean squared displacement, we square the average jump distance. The results are summarized in Table 6, where it is apparent that D estimated from eq 6 is within a factor of three of the calculated values for all cases. This level of qualitative agreement suggests that a jumping mechanism is primarily responsible for the penetrant diffusion. However, the quantitative differences also suggest that the

Table 6. Jump statistics for the penetrants in the different sized structures derived from the distributions for Figures 13−15. Numbers in parenthesis are error estimates, values for D in units of 1×10^{-5} cm²/s

			jump		D	
penetrant	structure size	residence time (ps)	time (ps)	distance (Å)	$\langle r^2\rangle f/6 \times 10^{-5}$ cm²/s	from trajectory $\times 10^{-5}$ cm²/s
He	125mer	52.1(31)	14.3(7.6)	12.7(7.0)	4.0	6.5
	729mer	54.6(29)	13.3(7.1)	13.1(7.0)	4.2	7.2
	2197mer	55.6(30)	13.4(7.4)	13.1(7.2)	4.1	6.1
Ar−He	125mer	84.1(66)	12.7(6.2)	8.8(4.6)	1.3	1.1
	729mer	71.1(61)	12.1(6.1)	9.1(4.7)	1.6	0.9
	2197mer	57.1(44)	11.7(5.9)	9.7(5.3)	2.3	1.2
CO_2−He	125mer	235(283)	11.6(6.0)	5.8(2.1)	0.23	0.11
	729mer	140(162)	11.1(6.5)	6.4(3.1)	0.45	0.12
	2197mer	128(146)	10.6(4.9)	6.3(2.9)	0.48	0.15

assumption of uncorrelated jump length and frequency, central to a successful application of transition state approaches, is not completely justifiable for the polymer−penetrant combinations considered here. Note that quantitative agreement is worse for the largest penetrant, which also supports this hypothesis.

IV. Conclusions

A definite system size effect is observed for the calculated excess chemical potential in united atom polypropylene glass. However, the effect on $\langle \mu^{ex} \rangle$ is significant only for "large" penetrants, such as CO_2−He and SF_6−He. In contrast, simulation size does not have a significant effect on the diffusive motion of any of the penetrants. Both the macroscopic diffusion coefficient and the local jump frequency and distance are essentially independent of structure size. Thus, for polymer glasses generated according to Gaussian statistics, large MD simulations are not required to study the diffusion of small penetrants. At least for the system sizes and penetrants studied here, the smallest simulations can be used without inducing significant error from size effects.

We also note the value of using the van Hove correlation function for calculating D and identifying statistical anomalies that can skew the data. With the limited MSD statistics available from MD simulations, it is important to analyze fully the data to prevent sampling artifacts due to poor statistics. Further, we note the importance of verifying the thermal control of the penetrants when performing simulations of small, weakly coupled systems such as the polymer/penetrant systems here.

Although penetrant motion is largely accomplished by a jump mechanism, polymer thermal motion at the segmental level correlates jump frequency and length, thus questioning the validity of the independence assumed in writing eq 6. For methods relying on static representations of the polymer glass, the presence of static, percolated networks through which the penetrant travels introduces length scales that lead to the influence of the simulation size on the value of D and the turnover distance not evident in full MD simulations. The fluctuations in the polymer cavity distribution in full MD simulations result in a dynamic network of diffusion pathways that lessen the influence of periodic boundary conditions. Thus, these results suggest the need to fully account for these dynamic pathways in transition state models for diffusion in glassy polymers.

Acknowledgment. We gratefully acknowledge the financial support provided by the Dow Chemical Co., the National Science Foundation Fellowship DGE-9253850, and Grant INT-9400209 and Delaware Research Partnership. We further thank the Cornell Theory Center, which received major funding from the National Science Foundation and New York State, the Advanced Research Projects Agency, the National Institute of Health, IBM Corp., and other member of the center's Corporate Research Institute, for the use of their facilities and equipment. We also wish to thank Dr. A. Gusev and Prof. Dr. U. Süter for useful discussions and the ETH-Zürich where part of this work was performed. The manuscript benefited from careful reviewing; we wish to thank the reviewers for their efforts.

References and Notes

(1) Tamai, Y.; Tanaka, H.; Nakanishi, K. *Macromolecules* **1994**, *27*, 4498.
(2) Mueller-Plathe, F. *Acta Polym.* **1994**, *45*, 259.
(3) Neogi, P., Ed. *Diffusion in Polymers*; Marcel Dekker: New York, 1996.
(4) Kotelyanskii, M. J.; Wagner, N. J.; Paulaitis, M. E. *J. Membr. Sci.* **1997**, *139*, 1.
(5) Mueller-Plathe, F. *J. Membr. Sci.* **1998**, *141*, 147.
(6) Takeuchi, H. *J. Chem. Phys.* **1990**, *93*, 2062.
(7) Mueller-Plathe, F.; Rogers, S. C.; van Gunsteren, W. F. *Macromolecules* **1992**, *25*, 6722.
(8) Mueller-Plathe, F. *J. Chem. Phys.* **1992**, *96*, 3200.
(9) Gusev, A. A.; Suter, U. W. *J. Chem. Phys.* **1993**, *99*, 2228.
(10) Mueller-Plathe, F.; Rogers, S. C.; van Gunsteren, W. F. *J. Chem. Phys.* **1993**, *98*, 9895.
(11) Mueller-Plathe, F.; Laaksonen, L.; van Gunsteren, W. F. *J. Mol. Graphics* **1993**, *11*, 118.
(12) Pant, P. V.; Boyd, R. H. *Macromolecules* **1993**, *26*, 679.
(13) Han, J.; Boyd, R. H. *Macromolecules* **1994**, *27*, 5365.
(14) Gee, R. H.; Boyd, R. H. *Polymer* **1995**, *36*, 1435.
(15) Gusev, A. A.; Suter, U. W.; Moll, D. J. *Macromolecules* **1995**, *28*, 2582.
(16) Han, J.; Boyd, R. H *Polymer* **1996**, *37*, 1979.
(17) Takeuchi, H.; Okazaki, K. *Mol. Simulation* **1996**, *16*, 59.
(18) Fukuda, M.; Kuwajima, S. *J. Chem. Phys.* **1997**, *107*, 2149.
(19) Fukuda, M.; Kuwajima, S. *J. Chem. Phys.* **1998**, *108*, 3001.
(20) Fried, J. R.; Goyal, D. K. *J. Polym. Sci.: Part B* **1998**, *36*, 519.
(21) Widom, B. *J. Chem. Phys.* **1963**, *39*, 2808.
(22) Mueller-Plathe, F. *Macromolecules* **1991**, *24*, 6475
(23) Deitrick, G. L.; Scriven, L. E.; Davis, H. *J. Chem. Phys* **1989**, *90*, 2370.
(24) Cuthbert, T. R.; Wagner, N. J.; Paulaitis, M. E. *Macromolecules* **1997**, *30*, 3058.
(25) Gray-Weale, A. A.; Henchman, R. H.; Gilbert, R. G.; Greenfield, M. L.; Theodorou, D. N. *Macromolecules* **1997**, *30*, 7298.
(26) Greenfield, M. L.; Theodorou, D. N. *Mol. Sim.* **1997**, *19*, 329.
(27) Sok, R. M.; Berendsen, H. J. C.; van Gunsteren, W. F. *J. Chem. Phys.* **1992**, *96*, 4699.
(28) van der Vegt, N. F. A.; Briels, W. J.; Wessling, M.; Strathmann, H. *J. Chem. Phys.* **1996**, *105*, 8849.
(29) Theodorou, D. N.; Suter, U. W. *Macromolecules* **1985**, *18*, 1467.
(30) Khare, R.; Paulaitis, M. E.; Lustig, S. R. *Macromolecules* **1993**, *26*, 7203.
(31) Kotelyanskii, M. J.; Wagner, N. J.; Paulaitis, M. E. *Macromolecules* **1996**, *29*, 8497.

(32) Gusev, A. A.; Mueller-Plathe, F.; van Gunsteren, W. F.; Suter, U. W. *Adv. Polym. Sci.* **1994**, *116*, 209.
(33) Weber, H.; Paul, W. *Phys. Rev. E* **1996**, *54*, 3999.
(34) Chitra, R.; Yashonath, S. *J. Chem. Phys. B* **1997**, *101*, 5437.
(35) Gusev, A. A.; Arizzi, S.; Suter, U. W.; Moll, D. J. *J. Chem. Phys.* **1993**, *99*, 2221.
(36) Sylvester, M. F.; Yip, S.; Argon, A. S. in *Computer Simulation of Polymers*; Prentice Hall: Englewood Cliffs, NJ, 1991; pp 105−140.
(37) Weiner, S. J.; Kollman, P. A.; Case, D. A.; Singh, U. C.; Ghio, C.; Alagona, G.; Profeta, S.; Weiner, P. *J. Am. Chem. Soc.* **1984**, *106*, 765.
(38) Plimpton, S.; Hendrickson, B. *J. Comput. Chem.* **1996**, *17*, 326.
(39) Plimpton, S. *J. Comput. Phys.* **1995**, *117*, 1.
(40) Hirschfelder, J. O.; Curtiss, C. F.; Bird, R. B. *Molecular Theory of Gases and Liquids*; John Wiley and Sons, Inc.: New Yor, 1954.
(41) Cheng, A.; Merz, K., Jr. *J. Phys. Chem.* **1996**, *100*, 1927.
(42) McQuarrie, D. A. *Statistical Mechanics*; Harper Collins: New York, 1976.

MA980997E